

INFLUENCE OF SWEEPBACK ON LEADING-EDGE VORTEX STABILIZATION

Heather R. Beem¹, David E. Rival^{1,2} and Michael S. Triantafyllou¹

¹Department of Mechanical Engineering
Massachusetts Institute of Technology
77 Massachusetts Avenue, Cambridge, MA 02139 USA
beem@mit.edu, mistetri@mit.edu

²Department of Mechanical and Manufacturing Engineering
University of Calgary
2500 University Dr NW, Calgary, AB, Canada T2N 1N4
derival@ucalgary.ca

ABSTRACT

The sweepback geometry characteristic of fish-like tails has been found to be insufficient for the stabilization of leading-edge vortices (LEVs) during unsteady motion. Direct force measurements and experimental visualizations, which include Particle Image Velocimetry (PIV) and Lead Precipitation, suggest that despite a strong spanwise flow in the LEV core at higher sweepback angles, the vortex breaks off and convects downstream at nearly the same time as for angles with little spanwise contribution. Despite the LEV's insensitivity to spanwise flow, the LEV and tip vortex were observed to maintain a stronger connection with one another at higher sweepback angles. This result implies that despite similar net performance for low and high sweepback angles alike, the resulting vortex-wake topologies varies dramatically from one another.

INTRODUCTION

Depending on the orientation and spatial-temporal scales of an unsteady manoeuvre or gust, it is not uncommon for the local angle of incidence of lifting bodies to rapidly vary and thus experience a dynamic-stall event, as described by McCroskey (1982). During such an event, the boundary-layer separation moves rapidly forward to the leading edge, at which point the bulk vortex dynamics are found to be insensitive to Reynolds number. In general, this dynamic-stall process leads to the formation of large separated vortical structures, e.g. leading-edge vortices (LEVs) around the lifting surface, thus increasing the loadings tremendously. Since the pioneering work by Ellington et al. (1996) on LEV formation in insect flight, a great deal of speculation has developed regarding the specifics of this particular three-dimensional dynamic-

stall process and its associated vortex topology. Here are some of the immediate questions that arise: What is the time scale associated with the variation in tip-vortex circulation during a gust-induced change in lift? In such unsteady cases do the bound and tip vortices vary proportionally in strength to one another? Can such vortex dynamics be used advantageously to deal with these rapid changes in the boundary conditions?

When observing efficient aquatic locomotion in nature, for instance the propulsion through oscillating tail fins as discussed by Triantafyllou et al. (2000), a swept planform is found to be the prevalent shape of most fins. However, the specific fluid-dynamic role of this planform during oscillatory motions has yet to be properly investigated. Under steady conditions, the effect of sweepback on lift enhancement through leading-edge vortex (LEV) stabilization is well understood, particularly in the context of delta-wing aircraft, as discussed by Polhamus (1971). When considering the possibility of spanwise vortex stabilization, Ellington et al. (1996) were the first to observe this phenomenon for the case of a flapping model-hawkmoth wing ($Re \approx 100$). They postulated that the spanwise flow through the vortex core, causing a conical spiral vortex, was responsible for the redirection of momentum towards the wing tip. This would then allow the LEV to remain sufficiently small for attachment, similar to the quasi-steady stabilization experienced in the delta-wing LEV arrangement. Not long after Ellington's study, Birch and Dickinson (2001) observed the stable LEV attachment on a fruit-fly wing ($Re \approx 115$) and proposed that this stabilization was instead due to the downward flow induced by the tip vortex, thus reducing the effective angle of attack. However, this is speculative and has yet to be quantified. Most recently, Lentink and Dickinson (2009) have shown that the LEV can be stabilized through a sweeping motion where centripetal and Corio-

lis accelerations play a dominant role. These studies were performed in the Reynolds number range of $100 \leq Re \leq 15,000$.

More abstract studies including those performed by Parker et al. (2007), Buchholz and Smits (2008), Kim and Gharib (2010) and Suryadi et al. (2010) have considered the unsteady separation behavior on dynamic, low-aspect ratio planforms. To some degree these studies have identified the influence of the wing-tip vortex on the development of the LEV, where a reduction or even complete elimination of the local separation is observed. However, most of these experiments have been limited in their findings since they have not provided information regarding the transfer of vorticity in the spanwise direction. Therefore a clear understanding of the vortex dynamics could not be quantified.

The present study simplifies the investigation of spanwise flow on LEV stabilization by eliminating geometric and kinematic factors that could unintentionally contribute to the vortex dynamics at hand. In isolation, the sweepback parameter generates a spanwise flow that should force vorticity towards the tip and allow for a greater stabilization of the LEV during rapid changes in incidence. In this way, the effect of spanwise flow on vortex formation on a high-aspect ratio wing can be isolated without the complication of other competing accelerations due to Coriolis forces, centripetal forces, etc.

BACKGROUND

Consider the vorticity equation for an incompressible, barotropic fluid with conservative body forces:

$$\frac{\partial \vec{\omega}}{\partial t} + (\vec{v} \cdot \nabla) \vec{\omega} = (\vec{\omega} \cdot \nabla) \vec{v} + \nabla \times \left(\frac{\vec{\nabla} \cdot \vec{\tau}}{\rho} \right), \quad (1)$$

where the terms on the right-hand-side of the equation represent the stretching/tilting of vorticity due to velocity gradients and the diffusion of vorticity due to viscous effects, respectively. The latter will be neglected here based on the argument that the time scales associated with LEV evolution are much more rapid than those for diffusion.

To further simplify, one can approximate the LEV as a vortex line running along the span of the wing, theoretically linking to the tip vortex so as to satisfy Helmholtz' vortex laws. Considering a slice through the LEV away from the tip in a cartesian coordinate system aligned with the vortex line such that x runs in the chordwise direction, y is normal to the wing and z is in the direction of the tip, one can write:

$$\frac{\partial \omega_z}{\partial t} + u \frac{\partial \omega_z}{\partial x} + v \frac{\partial \omega_z}{\partial y} + w \frac{\partial \omega_z}{\partial z} = \omega_z \frac{\partial u}{\partial z} + \omega_z \frac{\partial v}{\partial z} + \omega_z \frac{\partial w}{\partial z}. \quad (2)$$

However, when considering the advective terms the spanwise velocity component w in the vicinity of the vortex line can be assumed to dominate, such that $w \gg u$ and $w \gg v$. When considering the vortex stretching terms on the right-hand side, the gradients of velocity in x and y directions can also be neglected. Therefore one can hypothesize that for the case of rapid LEV formation in a strong spanwise flow the vorticity

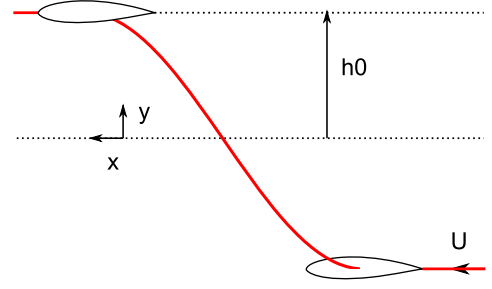


Figure 1. Schematic depicting the lateral motion, where h_0 is the amplitude and U is the towing velocity.

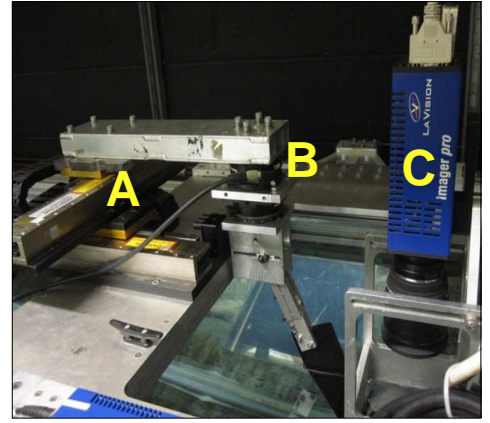


Figure 2. Experimental setup with linear motor for lateral motion (A), 6-component load cell with sweep-angle adjustment below (B), and moving PIV camera (C).

balance will be governed by:

$$\frac{\partial \omega_z}{\partial t} + w \frac{\partial \omega_z}{\partial z} = \omega_z \frac{\partial w}{\partial z}. \quad (3)$$

Therefore one can postulate that for larger sweepback configurations, an equilibrium state should be possible such that the vorticity produced at the leading edge is rapidly advected away towards the tip. This should serve to drain the vorticity away from the LEV so as to keep it at a manageable size and therefore fixed to the wing. Simultaneously to this spanwise advection, it can be argued that vortex stretching might also play an important role in LEV stabilization. In the current study, an initial investigation to identify the potential stabilization process of the LEV has been performed. In the following, the experimental techniques to characterize this behavior are presented.

EXPERIMENTAL SETUP

LEVs were generated on a NACA 0012 wing with rectangular planform by plunging the wing at $\alpha = 0^\circ$ in a single sideward motion while towing steadily down the length of the water tank; see Figure 1. The wing chord had dimensions of $c = 70\text{mm}$ with a span of $s = 420\text{mm}$. The plunge motion was modeled as one half wavelength of a sinusoidal motion corre-

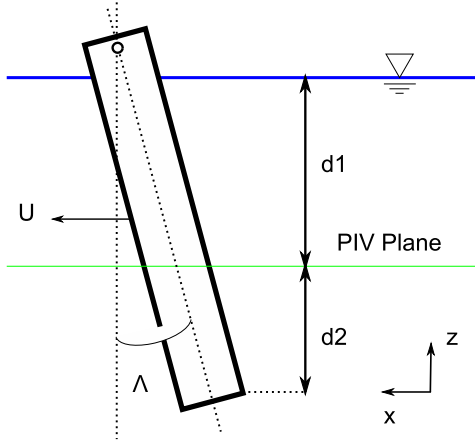


Figure 3. Schematic depicting the parameter space for the sweepback experiments, where U is the towing velocity, Λ is the sweepback angle and the ratio $d_1/(d_1 + d_2)$ defines the spanwise position of the PIV plane.

sponding to a Strouhal number of $St = fU/d = 0.3$, where f is the frequency of the motion and the towing speed was set to $U = 0.2m/s$ ($Re = 14,000$). The characteristic wake width was $d = 140mm$, chosen as twice the lateral-motion amplitude and wing chord ($d = 2h_o = 2c$) such that:

$$h(t) = h_o \cos(2\pi ft), \quad (4)$$

The lateral motion $h(t)$ was carried out using a single linear motor and was repeated for a range of low and high sweepback angles ($0^\circ \leq \Lambda \leq 45^\circ$).

Direct force measurements were acquired using a ATI Gamma six-axis load cell. A National Instruments USB-6218 data acquisition system was used to collect the amplified sensor output at 1000Hz. These values were calculated using the physical chord (c) and the effective span (s'), where $s' = s/\cos(\Lambda)$. The data was filtered using a Chebychev filter and were ensemble averaged over 10 runs. Inertial forces were on the order of 10% of the total force and were removed by estimating the model's mass and acceleration during the lateral motion. Figure 2 shows the general positioning of the load cell, drive system, and camera.

Visualizations using Particle Image Velocimetry (PIV) were performed at sweepback angles ($\Lambda = 15^\circ$) and ($\Lambda = 45^\circ$) at both inboard and outboard locations corresponding to 75%-span and 95%-span locations. The span location (%s) is defined here as the ratio of the normal distance from the free surface to the plane of interest (d_1) to the total distance to the tip ($s' = d_1 + d_2$). Refer to Figure 3 for a clear representation of the PIV plane definition. A Nd:YLF laser ($\lambda = 527nm$) was synchronized with a high-speed camera at a frequency of 600Hz in single-frame mode, which was towed with the wing, as shown in Figure 4. Velocity vector fields were calculated using an adaptive-correlation with 128x128 pixel and then 64x64 pixel interrogation windows, both with 50% overlap. Finally, light smoothing was carried out using a 3x3 filter.

In order to gain a global view of the vortex structures, Lead Precipitation was used for flow visualization. This technique uses an electrolytic reaction to produce lead flakes that

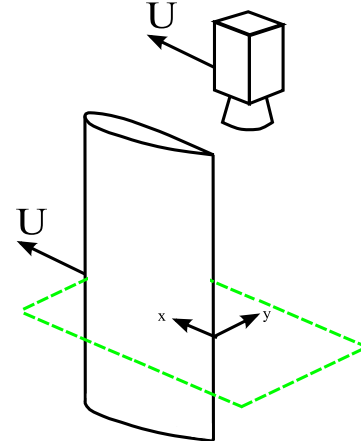


Figure 4. Schematic depicting relative position of the moving camera/wing system, where U is the towing velocity.

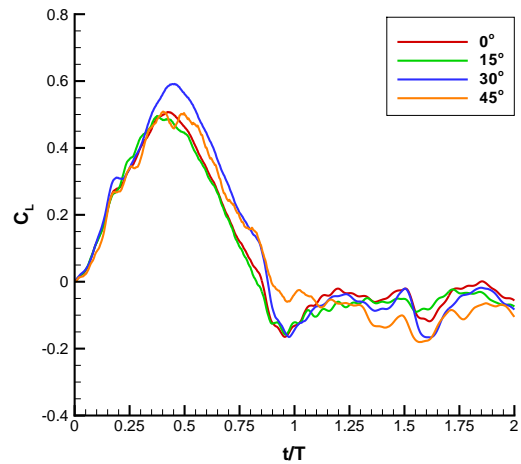


Figure 5. Time-dependent variation of the lift coefficient for various sweepback angles, where $t/T = 0$ and $t/T = 1$ represent the beginning and end of the lateral motion, respectively.

get caught in the boundary layer. A 10mm wide strip of lead tape was placed near the leading edge of the wing towards the pressure side where the LEV forms. Just on the opposite side, near the leading edge of the wing, a copper tape of the same size was placed to act as a cathode. A differential voltage was placed across these two strips (40V), and table salt was added to the water tank to complete the electrical path. The same laser used for the PIV measurements was also used to illuminate the lead precipitate at 25 Amps of current. Instead of a thin horizontal sheet, a volume of laser light was created by sending a loosely-focused laser beam through a cylinder lens thus expanding it into a thick vertical sheet to illuminate the entire region of interest. Images were recorded using a Canon EOS Rebel T2i camera with hi-definition video at 30 frames per second, providing a qualitative description of the three-dimensional vortex system.

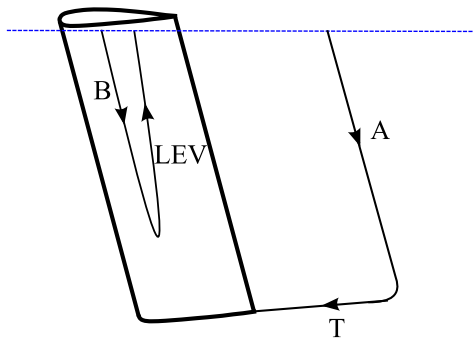


Figure 6. Resulting vortex topology at $t/T = 1$ for low sweepback cases (here $\Lambda = 15^\circ$), where A, B, T and LEV represent the starting, stopping, tip and LEV vortices in the wake, respectively. Arrows indicate direction of vorticity.

RESULTS

Lift coefficients corresponding to the hydrodynamic lift forces on the foil are shown in Figure 5. The start and end of the translatory motion is designated by $t/T = 0$ and $t/T = 1$, respectively. All sweepback angles tested, $\Lambda = 0^\circ$, 15° , 30° and 45° , show similar variations in lift, which suggests that the LEV is rapidly convected away soon after the mid-stroke position ($t/T = 0.5$) for all cases. The $\Lambda = 30^\circ$ sweepback angle demonstrates a slightly higher peak in lift, and the $\Lambda = 45^\circ$ sweepback angle demonstrates a slightly more sustained value, indicating a minor degree of LEV stabilization, but not significantly so.

In order to track the evolution of the LEV during the lateral motion, PIV measurements were performed for two sweepback cases, $\Lambda = 15^\circ$ and 45° , representing cases of mild and strong spanwise velocity components, respectively. Figures 8 and 9 display contours of non-dimensional vorticity associated with inboard (75%-span) and outboard (95%-span) measurement planes during distinct steps of the motion. The leading edge of the wing starts in the upper right corner of the frame ($x/c = y/c = 0$) at the beginning of the motion and traverses to the left to its end position ($x/c = -2$, $y/c = 0$). By the halfway point in the translatory motion ($t/T = 0.5$), the formation of a coherent LEV structure is evident for both sweepback angles at the inboard position; see Figure 8. Here the LEV is found to subsequently grow in size and strength, while moving downstream in the chordwise direction. In Figure 9, at the outboard measurement plane, a similar behavior is observed for the $\Lambda = 45^\circ$ case. In stark contrast, however, the out-of-plane vorticity for the $\Lambda = 15^\circ$ case is weak, suggesting a fundamental difference in the LEV formation towards the wing tip.

In order to properly ascertain the vortex topology for both low and high sweepback cases, Lead Precipitation visualizations were performed on both suction and pressure sides of the wing, shown in Figures 10 and 11, respectively. For the low sweepback angles, $\Lambda = 0^\circ$ and 15° , the LEV and tip vortices are weakly connected; see Figure 6. However, for higher sweepback angles, $\Lambda = 30^\circ$ and 45° , the LEV wraps strongly together with the tip vortex, as shown in Figure 7.

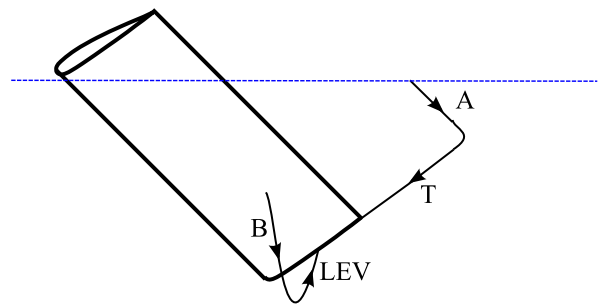


Figure 7. Resulting vortex topology at $t/T = 1$ for high sweepback cases (here $\Lambda = 45^\circ$), where A, B, T and LEV represent the starting, stopping, tip and LEV vortices in the wake, respectively. Arrows indicate direction of vorticity.

CONCLUSIONS

In this study, the dynamics of LEVs have been found to change very little with sweepback angle, which is directly correlated with the strength of the spanwise flow. This suggests that little stabilization occurs for such a fish-like tail geometry, and is evidenced primarily by direct, time-resolved force measurements. PIV and Lead Precipitation visualizations show that despite the lack of LEV stabilization, dramatic differences in the wake topology occur for these varying cases. At low sweepback angles, the induced flow from the tip vortex prevents separation such that the LEV and tip vortex demonstrate a weak connection with one another. In stark contrast to this gap region between LEV and tip vortex at low sweepback angles, high sweepback angles show no sign of disconnection and therefore form more obvious vortex-ladder type wake as observed in nature.

REFERENCES

- Birch, J. M., Dickinson, M. H., 2001, "Spanwise Flow and the Attachment of the Leading-Edge Vortex on Insect Wings," *Nature*, Vol. 412, pp. 729-733.
- Buchholz, J. H. J., Smits, A. J., 2008, "The wake structure and thrust performance of a rigid low-aspect-ratio pitching panel," *Journal of Fluid Mechanics*, Vol. 603, pp. 331-365.
- Ellington, C. P., van den Berg, C., Willmott, A. P., Thomas, A. L. R., 1996, "Leading Edge Vortices in Insect Flight," *Nature*, Vol. 384, pp. 626-630.
- McCroskey, W. J., 1982, "Unsteady Airfoils," *Annual Review of Fluid Mechanics*, Vol. 14, pp. 285-311.
- Parker, K., von Ellenrieder, K. D., Soria, J., 2007, "Morphology of the forced oscillatory flow past a finite-span wing at low Reynolds number," *Journal of Fluid Mechanics*, Vol. 571, pp. 327-357.
- Polhamus, E. C., 1971, "Predictions of Vortex-Lift Characteristics by a Leading-Edge Suction Analogy," *Journal of Aircraft*, Vol. 8, pp. 193-199.
- Suryadi, A., Ishii, T., Obi, S., 2010, "Stereo PIV measurement of a finite, flapping rigid plate in hovering condition," *Experiments in Fluids*, Vol. 49, Number 2, pp. 447-460.
- Triantafyllou, M. S., Triantafyllou, G. S., Yue, D. K. P., 2000, "Hydrodynamics of Fishlike Swimming," *Annual Review of Fluid Mechanics*, Vol. 32, pp. 335-353.

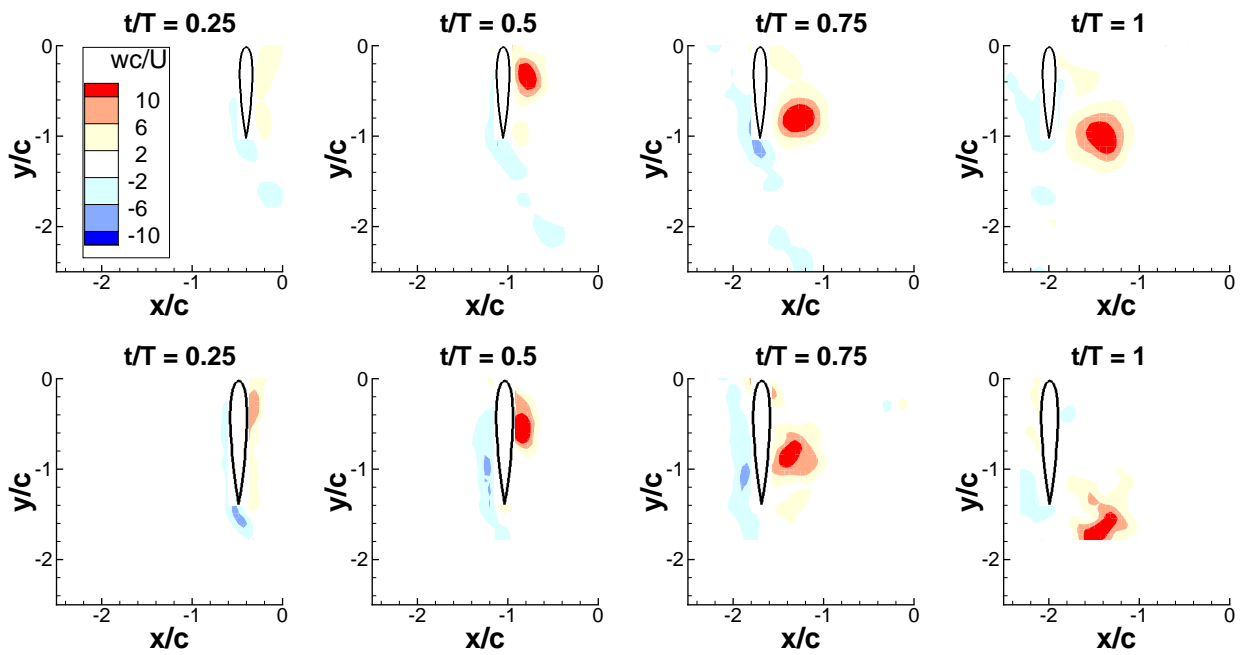


Figure 8. Cross-section of the LEV evolution at the 75%-span position through four time steps in the plunge cycle for $\Lambda = 15^\circ$ (top row) and $\Lambda = 45^\circ$ (bottom row). Note that the axes are non-dimensionalized with the chord ($c=70\text{mm}$).

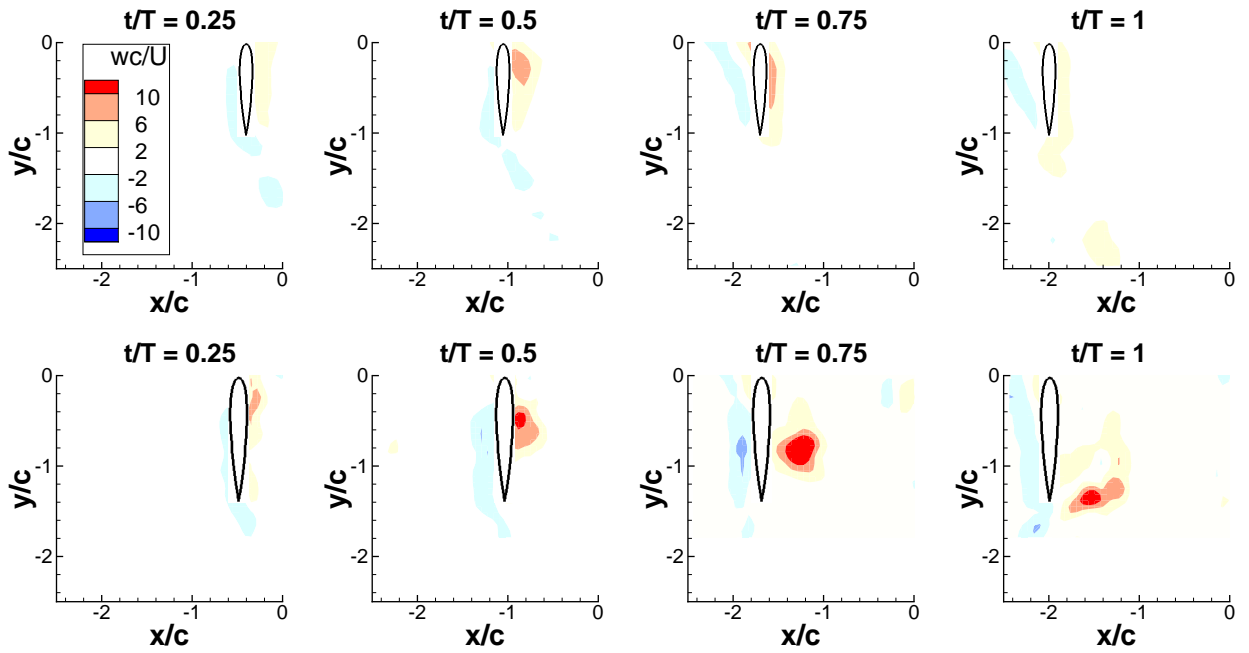


Figure 9. Cross-section of the LEV evolution at the 95%-span position through four time steps in the plunge cycle for $\Lambda = 15^\circ$ (top row) and $\Lambda = 45^\circ$ (bottom row). Note that the axes are non-dimensionalized with the chord ($c=70\text{mm}$).

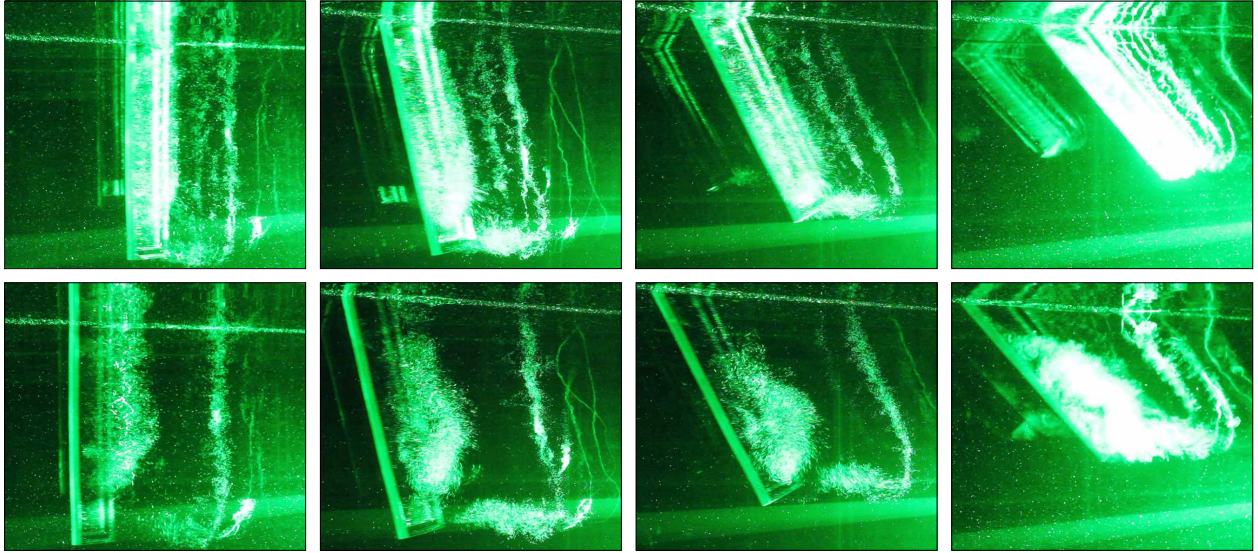


Figure 10. Lead Precipitation visualizations on wing suction side during second half of lateral motion; from left to right sweepback angles of $\Lambda = 0^\circ, 15^\circ, 30^\circ$ and 45° at $t/T = 0.75$ (top row) and $t/T = 1$ (bottom row).

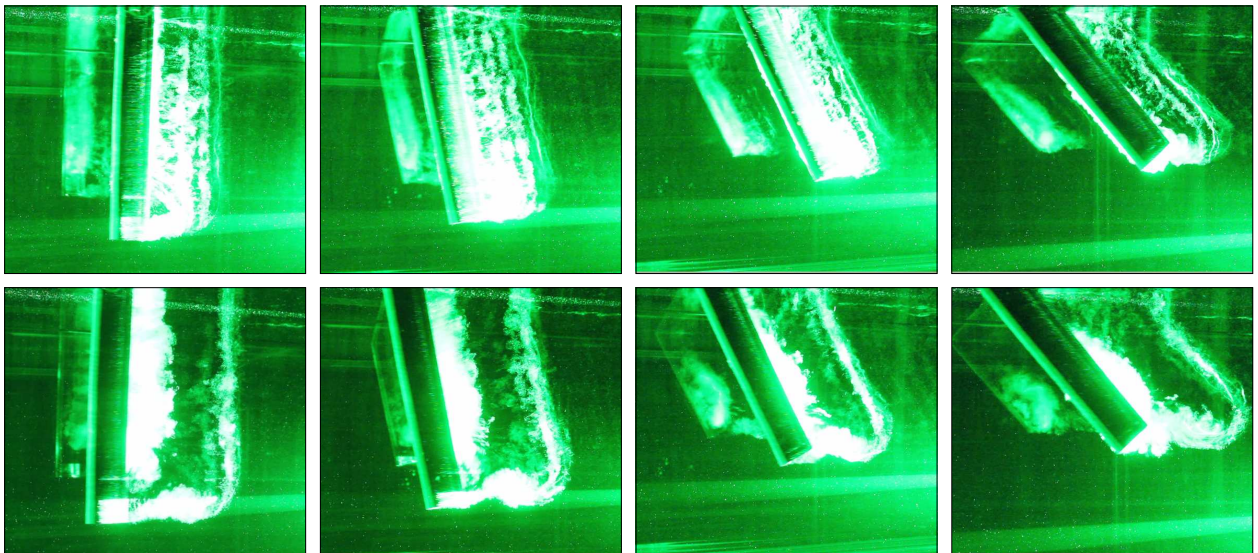


Figure 11. Lead Precipitation visualizations on wing pressure side during second half of lateral motion; from left to right sweepback angles of $\Lambda = 0^\circ, 15^\circ, 30^\circ$ and 45° at $t/T = 0.75$ (top row) and $t/T = 1$ (bottom row).